ADVANCED MATERIALS
www.advmat.de

Magnetic Dynamic Polymers for Modular Assembling and Reconfigurable Morphing Architectures

Xiao Kuang, Shuai Wu, Qiji Ze, Liang Yue, Yi Jin, S. Macrae Montgomery, Fengyuan Yang, H. Jerry Qi, and Ruike Zhao**

Shape-morphing magnetic soft materials, composed of magnetic particles in a soft polymer matrix, can transform shape reversibly, remotely, and rapidly, finding diverse applications in actuators, soft robotics, and biomedical devices. To achieve on-demand and sophisticated shape morphing, the manufacture of structures with complex geometry and magnetization distribution is highly desired. Here, a magnetic dynamic polymer (MDP) composite composed of hard-magnetic microparticles in a dynamic polymer network with thermally responsive reversible linkages, which permits functionalities including targeted welding for magnetic-assisted assembly, magnetization reprogramming, and permanent structural reconfiguration, is reported. These functions not only provide highly desirable structural and material programmability and reprogrammability but also enable the manufacturing of functional soft architected materials such as 3D kirigami with complex magnetization distribution. The welding of magnetic-assisted modular assembly can be further combined with magnetization reprogramming and permanent reshaping capabilities for programmable and reconfigurable architectures and morphing structures. The reported MDP are anticipated to provide a new paradigm for the design and manufacture of future multifunctional assemblies and reconfigurable morphing architectures and devices.

1. Introduction

Shape-morphing materials capable of altering the structural geometry upon external stimuli, such as heat, light, and magnetic field, find diverse applications in actuators,[1] soft robots,[2] flexible electronics,[3] and biomedical devices.[4] Various stimuli-responsive smart materials, including shape memory polymers,[5] hydrogel composites,[6] liquid crystal elastomers,[7] and magnetic soft materials (MSMs),[8] have been implemented. In particular, MSMs, composed of hard-magnetic materials in a soft polymer matrix, enable remote, fast, and reversible shape morphing, and have attracted increasing attention in applications such as soft robots for minimally invasive surgery,[9] where the actuation in confined and enclosed spaces is required. The magnetically actuated shape-morphing is a result of the interactions between the MSM's magnetization (or ferromagnetic polarity) and the applied magnetic field. When the magnetization of embedded hard-magnetic particles is not aligned with the applied magnetic field, a body torque is exerted on the material and leads to a deformation that tends to align the magnetization with the magnetic field.[10] The on-demand shape morphing is determined by both the structural geometry and the magnetization distribution. Therefore, the manufacturing of structures with intricate geometry and magnetization distribution is highly desirable, which enables shape morphing in a programmable fashion.

From existing efforts, molding with template-assisted post magnetization is very commonly used to fabricate the geometry and magnetization distribution.[11] To enhance the material and structural programmability, various advanced manufacturing techniques, including ultraviolet lithography[12] and additive manufacturing,[13] have recently been developed to create complex shapes and magnetization distribution via physical alignment of magnetic dipoles followed by chemical curing of the matrix. For example, Kim et al.[13a] exploited the direct ink writing technique to manipulate the complex magnetization patterns in 3D printed MSMs for predetermined shape morphing. For the above methods, the magnetization is coupled with the manufacturing process, retarding the manipulation of the geometry and the magnetization distribution after manufacturing. In addition, it is still challenging to create 3D structures of complex shapes by directly 3D printing the magnetic composite. To tackle this issue, magnetic-assisted material assembling and magnetization reprogramming approaches

Dr. X. Kuang, Dr. L. Yue, S. M. Montgomery, Prof. H. J. Qi
The George W. Woodruff School of Mechanical Engineering
Georgia Institute of Technology
Atlanta, GA 30332, USA
E-mail: qih@me.gatech.edu
S. Wu, Dr. Q. Ze, Y. Jin, Prof. R. Zhao
Department of Mechanical and Aerospace Engineering
The Ohio State University
Columbus, OH 43210, USA
E-mail: zhao.2885@osu.edu
Prof. F. Yang
Department of Physics
The Ohio State University
Columbus, OH 43210, USA
The ORCID identification number(s) for the author(s) of this article can be found under https://doi.org/10.1002/adma.202102113.

DOI: 10.1002/adma.202102113

have been recently explored. In the magnetic-assisted material assembling, the intrinsic dipole–dipole interactions enable the self-organization of magnetic modules into larger 2D structures.[14] Modules with hard magnets as inclusions are often used to enhance the magnetic attraction force; however, it compromises the structure's overall flexibility and homogeneity, which is not preferred if magnetic actuation with complex shape morphing is needed.[14a,b] In general, most existing magnetic-assisted assemblies are based on physically attaching the magnetic modules to each other, which can be easily broken under external perturbation. There is one pioneering work that achieves assembly with bonding by thermoplastic or solder via thermal activation, but the material inhomogeneity introduced by the bonding materials may influence the actuation behavior.[15] Directly reprogramming magnetization distribution provides an alternative approach to post-manipulate actuation modes.[16] In this case, remagnetizing the composite using a large magnetic field above the coercivity of the magnetic material,[16a,b] or heating the magnetic material to above its Curie temperature to demagnetize before remagnetizing it[16c,d] are the most widely used methods. Another recently reported effort reprograms the magnetization by physically realigning the magnetic particles confined in fusible polymer microspheres that are embedded in a deformed elastomer matrix.[16e] Although reprogramming magnetization provides reconfigurable shape morphing, the material's function can still be limited by its unchangeable structural geometry. To the best of our knowledge, MSMs with a permanent shape reconfiguration capability are beyond the scope of existing studies.

2. Results and Discussion

In this work, we develop a magnetic dynamic polymer (MDP) composite that enables both structural and material programmability and reprogrammability with complex geometry and magnetization distribution for multifunctional and reconfigurable shape morphing. Inspired by active research in using covalent dynamic polymers (DPs) for materials welding and reprocessing,[17] we design the reprogrammable and reconfigurable morphing MDP consisting of hard-magnetic microparticles (NdFeB) and reversibly cross-linked DP matrix (**Figure 1**a). As a proof of concept, a DP matrix bearing thermally reversible Diels–Alder (DA) reaction between furan and maleimide is used. The maleimide and furan groups can proceed with forward DA reaction at low temperature to form adduct linkages, which can be cleaved via retro Diels–Alder (rDA) reaction upon heating.[18] The dynamically cross-linked DP and MDP can rearrange network topology by bond exchange reaction (BER) at a mild temperature (T_{BER}) and go through bond cleavage at elevated temperature (T_{rDA}), enabling the attractive property of heat-induced reversible elastic–plastic transition after material manufacturing (Figure 1b). The MDP integrates three functional properties, including: i) welding-enhanced assembling, ii) in situ magnetization reprogramming, and iii) remotely controlled permanent shape reconfiguration. We first illustrate the seamless welding of modules via forming new dynamic linkages at the interfaces to achieve modular assembling (Figure 1c). The welding function can be coupled with the magnetic-assisted assembly that will be discussed in the following section to enable complex shape-morphing structures. In addition, with the cleavage of linkages at T_{rDA}, a small magnetic field can chain up dipoles along the field direction for magnetization reprogramming, which further alters the shape morphing modes under the actuation magnetic field (Figure 1d). Meanwhile, simultaneous magnetic actuation and permanent structural reconfiguration of the DP matrix at mild temperatures (T_{BER}) allow remote reshaping of the material into a new stress-free architecture (Figure 1e). Besides, the MDP-based materials and architectures with programmed shape and magnetization distributions are capable of fast and reversible morphing shapes under external magnetic fields at room temperature. The welding of magnetic-assisted modular assembly can be further combined with the magnetization reprogramming and the reshaping capabilities for programmable and reconfigurable architectures and morphing structures.

To prepare the DP matrix, a furan-grafted prepolymer is first synthesized by the ring-opening reaction between an epoxy oligomer and furfurylamine. The prepolymer chains have an average of 13 pending furan groups, as indicated by the gel permeation chromatography measurement (Figure S1, Supporting Information). The linear prepolymer is cross-linked by the bismaleimide cross-linker via DA reaction, forming thermally reversible adduct linkages, as evidenced by Fourier transform infrared (FTIR) spectroscopy (Figure S2, Supporting Information). The maleimide to furan ratio (r) is used to tune the mechanical property, network cross-linking density, and thermal property of DP (Figure S3, Supporting Information). The DP with $r = 0.15$ (Young's modulus of 106 ± 9 kPa and glass transition temperature of −35 °C) is selected for use in the rest the work reported here (**Figure 2**a). To prepare MDP, NdFeB microparticles with an average size of 25 μm are dispersed in the DP matrix. The unmagnetized particles with negligible interactions can be evenly dispersed in the matrix after curing, as the scanning electron microscopy (SEM) images indicate no apparent particle aggregation (Figure S4, Supporting Information). Note that the microparticle size does not prominently influence the actuation performance of MDP composites due to comparable mechanical properties (at strain <20%) and similar magnetic properties (Figure S5, Supporting Information). The DP and MDP are soft stretchable elastomers showing break strain over 200%. Young's modulus of MDP increases linearly from 106 to 515 kPa with NdFeB microparticles concentration varying from 0 to 20 vol% (Figure S5, Supporting Information). We choose the NdFeB microparticle concentration of 15 vol% to manufacture MDP considering the balanced actuation performance and material density for various 2D and 3D structure actuation. After manufacturing and post-magnetization, the obtained MDP shows Young's modulus of 400 ± 20 kPa. The magnetization of the post-magnetized MDP is 75 kA m^{-1} (Figure S6, Supporting Information), which is stable at room temperature.

Unlike conventional chemically cross-linked polymer and composites, DP network or covalent adaptable network polymer is a class of chemically cross-linked polymer with a sufficient amount of dynamic or exchangeable covalent bonds in the polymer network, which enables material flow and permanent shape change after activating the dynamic bonds.[17c,19] DP

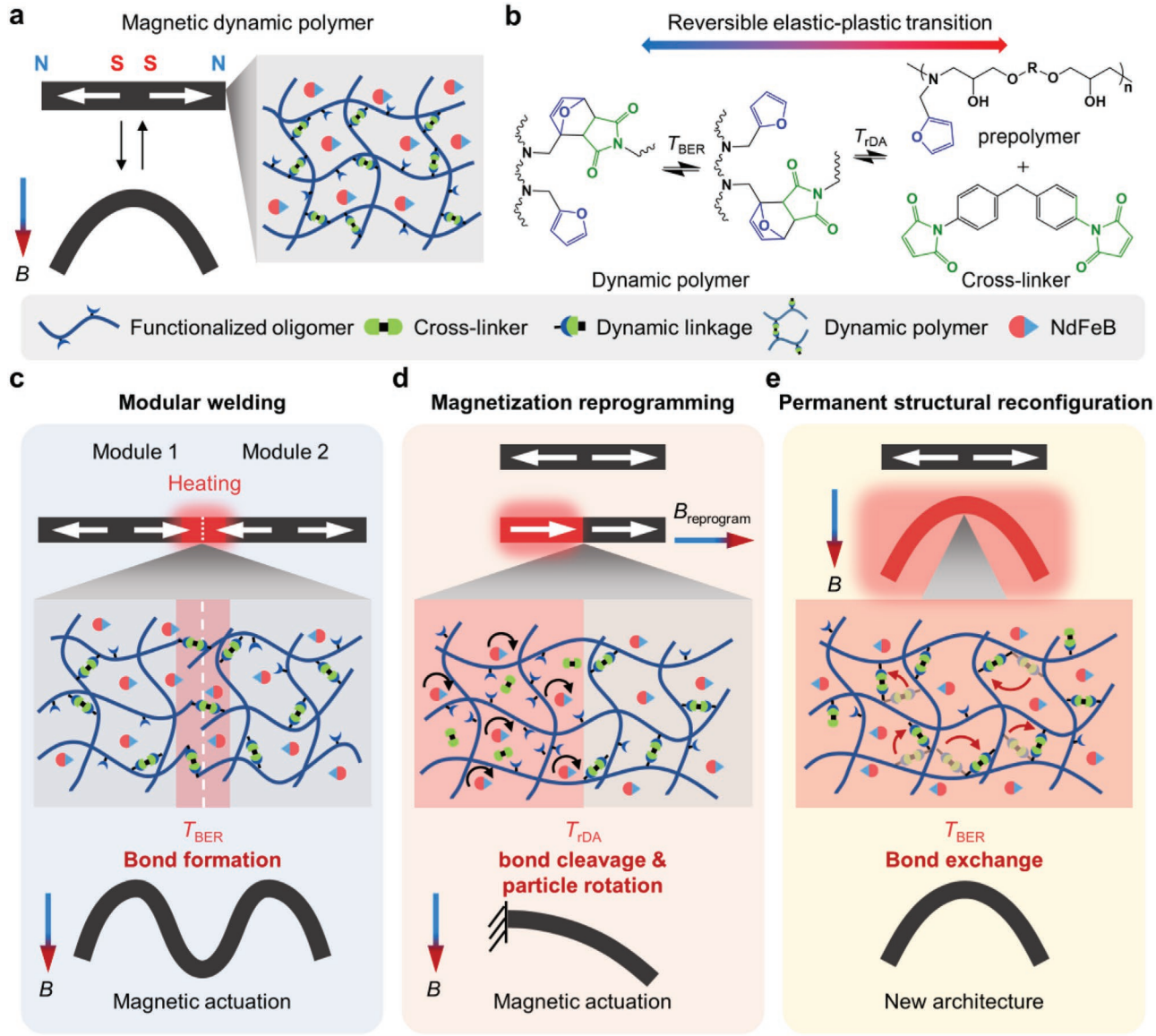

Figure 1. Schematics of the working mechanism and functions of the magnetic dynamic polymer (MDP). a) Schematics of the MDP composition. NdFeB microparticles are embedded in a dynamic polymer (DP) bearing reversible chemical bonds. b) Scheme of reversible elastic–plastic transition via network topology transition in the DA-reaction-based DP at different temperatures. The bond exchange reaction between free furan and DA adduct linkage for network arrangement is predominant at mild temperatures (T_{BER}), and reversible bond cleavage is favored at an elevated temperature (T_{rDA}). c) Schematics of modular welding of MDP modules at a temperature near T_{BER}. d) Schematics of magnetization reprogramming by bond cleavage and particle rotation under a magnetic field at T_{rDA}. e) Schematics of the magnetically guided permanent structural reconfiguration of MDP by plasticity via stress relaxation at T_{BER}.

networks possess desirable attributes of chemical cross-linking in thermosets and reprocessability in thermoplastics.[20] The fabricated DP and MDP here manifest heat-induced reversible elastic–plastic transition. At room temperature, DP and MDP show excellent elasticity and low hysteresis in the cyclic loading–unloading test (Figure S7, Supporting Information), due to low T_g and stable chemical linkages. This is also evidenced by a rubbery plateau from 25 to 80 °C by dynamic mechanical analysis (DMA) test (Figure 2b). The rubbery modulus of the MDP slightly decreases before 80 °C and sharply drops after 100 °C, owing to the cleavage of the dynamic linkages. Note that the MDP shows a larger high-temperature modulus and network stability than the DP due to the potential polymer-filler interaction. The underlining mechanism could be the interaction of the ethylene oxide backbone of the DP with the iron in NdFeB microparticle,[21] which still needs to be verified. Furthermore, creep tests are conducted at different temperatures and applied stress to reveal temperature-sensitive mechanical properties of the MDP. The apparent zero shear rate viscosity (η_0) of the chemically cross-linked network is obtained by the creep test (Figure S8, Supporting Information). The η_0 of the MDP decreases from nearly 10^9 Pa s at room temperature to 10^6 Pa s at 90 °C, showing prominent temperature-sensitive mechanical behaviors. Aside from the temperature-dependent

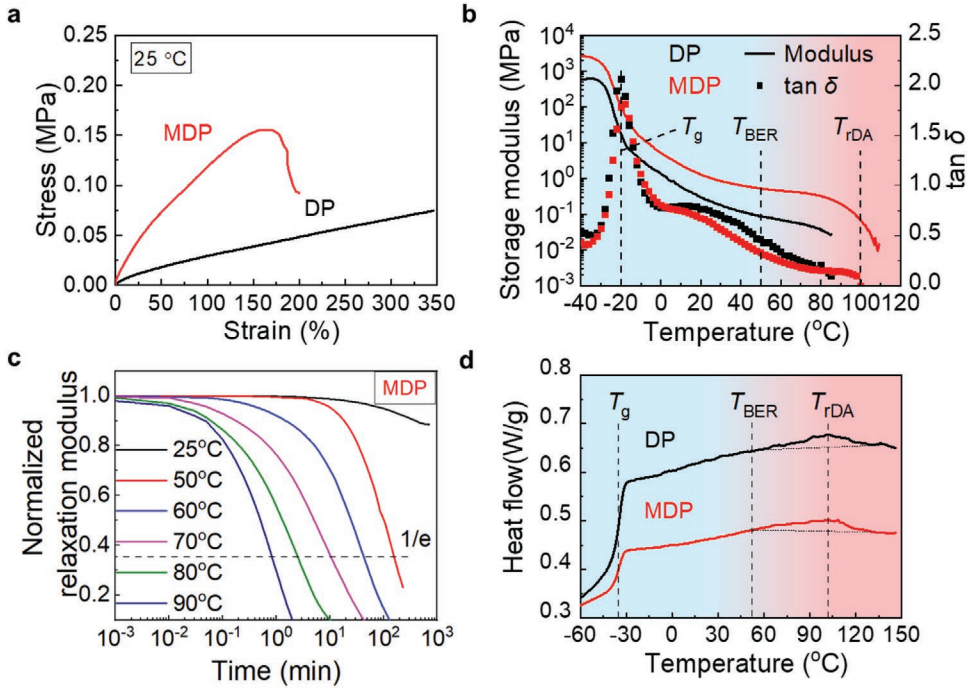

Figure 2. Mechanical and thermomechanical characterization of the DP and MDP. a) Tensile stress–strain curves of the DP and MDP. b) DMA heating curves for the DP and MDP from –40 to 120 °C with the marked characteristic glass transition temperature (T_g), bond exchange reaction temperature (T_{BER}), and rDA-reaction temperature (T_{rDA}). c) Normalized relaxation modulus as a function of time in the stress relaxation test of MDP at different temperatures. d) DSC heating curves of DP and MDP from –60 to 150 °C with marked characteristic temperatures.

mechanical properties, the network topology can also be rearranged via dynamic BER,[22] which is evaluated by the stress relaxation tests at various temperatures from 25 to 90 °C. Figure 2c shows the normalized relaxation modulus decreasing with time. At room temperature, the normalized relaxation modulus is nearly stable, indicating good geometry stability. By contrast, the stress relaxation process is accelerated when the temperature goes above 50 °C, leading to prominent material plasticity. The underlying mechanism for temperature-sensitive elastic–plastic transition upon heating is the network breaking and rearrangement via dynamic bond cleavage and exchange, respectively. To evaluate the temperature-variant bond breaking, differential scanning calorimetry (DSC) tests are conducted. On the DSC heating curves, an endothermal peak ranging from 50 to 120 °C is observed in both the DP and the MDP due to continuous bond-breaking via rDA reaction (Figure 2d). The rDA reaction degree as a function of temperature is semi-quantitatively evaluated by the normalized areal integration under the endothermal peak of the DSC heating curve (Figure S9, Supporting Information). A gel point conversion ($p_{gel} \approx 74\%$) is predicted between 80 and 90 °C (see Supporting Information, DP network relaxation analysis). The peak temperature at around 100 °C suggests the fastest bond-breaking rate, which is denoted as rDA temperature (T_{rDA}). It is noted that the cleaved linkages can reform upon cooling and annealing as supported by FTIR (Figure S2c, Supporting Information). On the basis of the reversible elastic–plastic transition of the MDP, shape and magnetization can be manipulated by corporative control of temperature and magnetic field for multifunctional reconfigurable morphing architectures.

We first demonstrate the function of magnetic-assisted assembling by magnetic attraction and seamless welding of magnetic modules. **Figure 3**a shows the longitudinally magnetized rectangular magnetic modules automatically attach to each other rapidly (≈0.3 s) with good contact. Afterward, the assembly is treated at 80 °C for 5 min either by direct heating or infrared (IR) light (Figure S10, Supporting Information) to be welded into an intact part. As the BER between the contacting interfaces generates strong chemical bonding, the welded assembly can sustain large stretching without breaking (Video S1, Supporting Information). The welding efficiency is quantified by the tensile fracture strain ratio of the welded samples to the original one (Figure 3b). The welding efficiency is 75% at room temperature after 2 days due to the very slow dynamic exchange reaction and bond formation at room temperature (Figure 3c). When at 80 °C, the welding efficiency can increase to 82% for 5 min treating and 95% for 20 min.

We further extend this concept to the modular assembly of stable 2D structures with on-demand magnetization patterns and geometries using different modules. We achieve this by using two basic simple building modules: a square with single-directional magnetization (Module 1) and a square with bidirectional magnetization (Module 2) (Figure 3d). The magnetic attraction provides these two basic building modules with five different combination logics (Video S2, Supporting Information). Under certain boundary conditions, the response of these combination logics under an out-of-plane magnetic field generates twisting, bending, twisting–bending, bending–folding (same direction), and bending–folding (orthogonal direction), respectively. These logics can be further used to achieve more

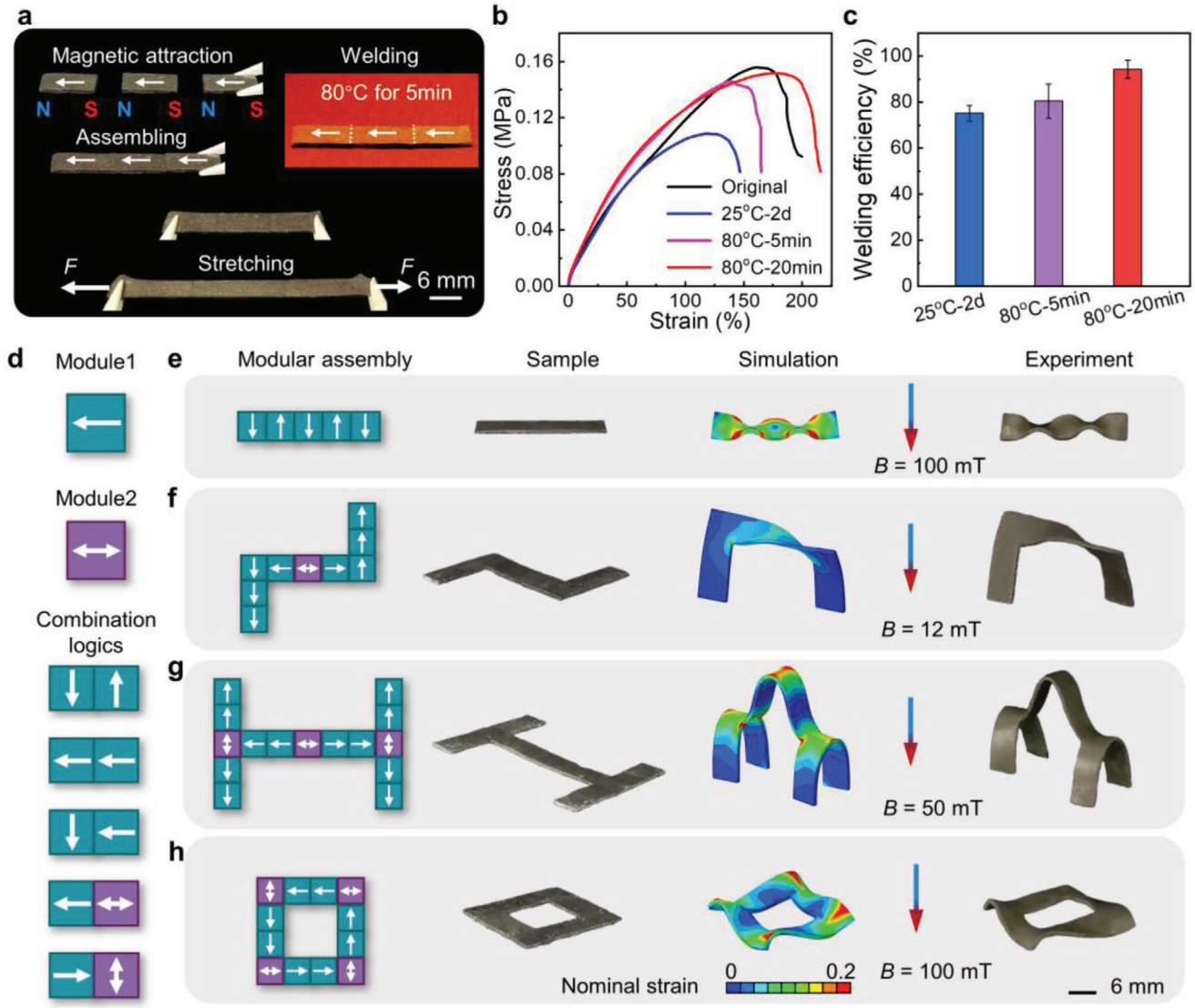

Figure 3. Magnetic-assisted modular assembling with seamless welding. a) Images of a long strip assembly consisting of three MDP modules via magnetic attraction followed by infrared (IR) light heating (80 °C for 5 min). b) Tensile stress–strain curves of the original sample and the welded MDP samples processed under different conditions. c) Effect of processing conditions on the welding efficiency of the processed MDP. d) Schematics of a square single-directional magnetization module and a bidirectional magnetization module with five double-unit combination logics via magnetic attraction. e–h) Schematic designs, finite-element analysis, and experimental results of various assembled 2D planar structures with programmed magnetization for complex shape morphing: a twisting strip (e), a "Z"-shaped structure (f), an "H"-shaped structure (g), and a square annulus structure (h).

intricate shape changes. For example, a strip with five pieces of Module 1 arranged in twisting logics is assembled and welded at 80 °C for 20 min. As shown in Figure 3e, the obtained straight strip assembly transforms to a twisting shape rapidly upon applying a magnetic field of 100 mT (see Figure S11, Supporting Information, for details of the electromagnetic coils) and quickly recovers its original shape upon the removal of the applied field (Video S2, Supporting Information). The shape morphing of the assembled MDP is predicted by finite-element analysis (FEA) through a user-defined element subroutine,[10] which guides the design of assemblies for target shape transformation under the application of magnetic fields. The simulation is conducted using the experimentally measured mechanical and magnetic properties, showing good agreement with the experimental result.

The logics presented above are further used to assemble the building modules into a rich set of more intricate 2D magnetization patterns on planar structures for complex shape morphing (Video S2, Supporting Information). In Figure 3f, the combination of bending, bending–folding (same direction), and bending–twisting logics is used to design a "Z"-shape structure for large twisting morphing under an applied magnetic field of 12 mT, as predicted by our FEA simulation. An "H"-shape structure is assembled by using 15 modules with only bending and bending–folding (both types) logics to generate large pop-up deformation under an external magnetic field of

50 mT as illustrated in Figure 3g. We also assemble a closed shape by using bending and bending–folding (both types), displaying an undulating shape morphing under a magnetic field of 100 mT (Figure 3h). The simulation results match the experimental results well, demonstrating that the modular assembly strategy can be assisted by FEA to design the shape-morphing architectures and their response under magnetic actuation. It is noted that the magnetization of each module is retained after welding. Our method of using the MDP for magnetic-assisted modular assembling with welding enables material integrity for complicated shape morphing, distinguishing from the existing magnetic-assisted assemblies based on physically attaching the magnetic modules (without chemical bonding).[14a,b] This assembly strategy of using the logics can achieve an almost unlimited number of possible shape morphing designs.

We also achieve in situ magnetization reprogramming via cleavage of dynamic linkages at elevated temperatures. To selectively reprogram the magnetization, photothermal heating by IR light illumination and photomasks are used (**Figure 4**a). Upon heating above T_{rDA}, the viscosity is reduced tremendously, and thus the magnetic particles can move freely in the MDP, leading to dipole realignment along an external magnetic field, which can be relocked after cooling. The realignment of NdFeB microparticles can alter the magnetization of reprogrammed MDP samples. Under the heating temperature of 110 °C and the magnetic field of 35 mT, the magnetization of reprogrammed MDP films with 45° orientation is nearly 83% of the initial magnetization (Figure S12, Supporting Information), which is sufficient for the magnetic actuation. Moreover, the reprogrammed remanent magnetization can be enhanced to nearly 100% by increasing the applied magnetic field to 140 mT. Cyclic reprogramming tests show, under a small magnetic field of 35 mT, that the remanent magnetization can be reversibly shifted from one direction to another for multiple cycles with some reduction. Similarly, by increasing the reprogramming field to 140 mT, nearly 100% of the initial magnetization can be obtained in at least three reprogramming cycles (Figure S12, Supporting Information). These results suggest excellent magnetic stability of the MDP composites during reprogramming. As an example, in Figure 4b, we fabricate a 4 × 4 MDP array encapsulated by silicone rubber to illustrate the selective magnetization reprogramming (Figure S13 and Video S3, Supporting Information). An aluminum foil as a photomask is used to enable local photothermal heating of

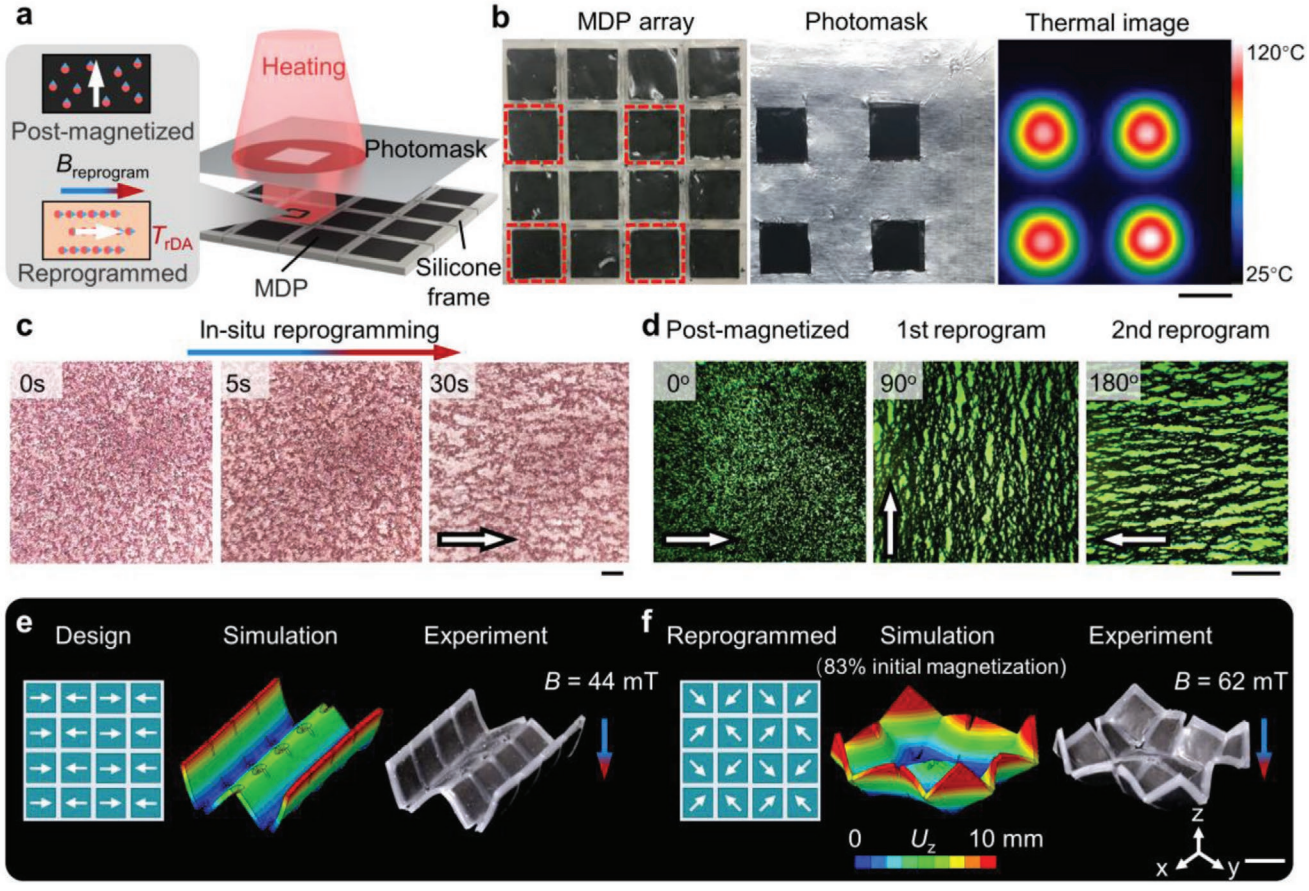

Figure 4. In situ reprogramming of magnetization in the MDP. a) Schematics of magnetization reprogramming of silicone encapsulated MDP array using an IR light source and a photomask under a magnetic field. The magnetic particles can be realigned by an external magnetic field at T_{rDA}. b) Image of an as-fabricated 4 × 4 MDP array, an aluminum photomask, and temperature profile after exposure to IR illumination. c) Microscopy snapshots of the in situ realignment of NdFeB particles in MDP at around 110 °C under a 35 mT magnetic field. d) Multiple cycles of magnetization reprogramming from the initial isotropic dispersion to chain-like structures along the external magnetic field direction. e,f) Designs, simulations, and experimental results of the MDP array with the initial magnetization (e) and reprogrammed magnetization (f). Scale bars in (c,d): 500 µm. Scale bars in (b,e,f): 10 mm.

selectively exposed MDP cells to 110–120 °C. The magnetic particles in the heated MDP cells physically rotate and reorient under a 35 mT homogenous magnetic field provided by a Halbach array magnet, which is sufficient to reprogram the magnetization to satisfy the actuation. The in situ dipole realignment is observed under digital microscopy coupled with a pair of electromagnetic coils (Figure S14, Supporting Information). As shown in Figure 4c, when the MDP viscosity reduces upon heating, the post-magnetized NdFeB particles first form small aggregation and rotate within 5 s and then tend to form a chain-like structure after 30 s under a 35 mT magnetic field (Video S3, Supporting Information). It is observed the presence of densely and evenly distributed chain-like structures does not lead to obvious anisotropic mechanical properties, as indicated by the tensile tests for the 0° and 90° reprogramming samples (Figure S15, Supporting Information). Due to the reversible elastic–plastic transition of MDP, the magnetization realignment can be repeated when sequentially applying external magnetic fields with different directions (Figure 4d). The alignment of NdFeB particles during reprogramming will induce chain-shape aggregation. But this aggregation becomes stable quickly and the MDP is capable of repetitive reprogramming while maintaining a stable dispersion and chain width (shown in Figure S16, Supporting Information). To test the efficacy of magnetization reprogramming, the planar 4 × 4 MDP array is initially magnetized horizontally in an alternating manner for each column of cells, as shown in Figure 4e. The 2D array morphs into a 3D "W" shape in a 44 mT out-of-plane magnetic field, which is well-captured by the FEA simulation. Next, a four-step reprogramming procedure is used to reprogram the selective MDP cells with four different reprogrammed magnetization directions, respectively (Video S3, Supporting Information). As shown in Figure 4f, the targeted reprogrammed magnetization has the polarity oriented in the diagonal of each cell pointing to the four centers. Upon applying a 62 mT out-of-plane magnetic field, the reprogrammed MDP array morphs into a 3D surface with four dents. The experimental result matches the simulation well using the measured magnetization (83% of the initial magnetization). It is noted that the thermally reversible reaction also enables hot recycling of MDP (by both solvent and hot-compression) (Figure S17, Supporting Information). The comparable mechanical properties of original and recycled materials for multiple cycles indicate the excellent thermal and mechanical stability of the MDP composite. It should be noted that a higher reprogramming resolution is feasible (such as at the millimeter-scale shown in Figure S18, Supporting Information). Compared with the existing magnetization reprogramming techniques using various magnetic soft composites, MDP offers the combined features of selective magnetization reprogramming under mild conditions, in situ reprogramming without mechanical folding, high remanent magnetization for efficient actuation, and high reprogramming resolution as well as enhanced sustainability.

The reshaping capability offered by the plasticity of the MDP can be harnessed to manufacture stress-free 3D intricate soft architectures with complex magnetization that would otherwise be very challenging to implement.[23] Multistable kirigami and origami tessellations with intrinsic structural buckling instability[24] find broad applications in morphing architectures and metamaterials with programmable complex geometries and novel mechanical properties. Advances have been made by several groups for soft robotics and active metamaterials via controllable magnetic-driven buckling deformations.[11b,16f,23,25] In **Figure** 5a, a planar kirigami design with four helical cuts (or helical design) is first molded and then post-magnetized in its mechanically stretched-out configuration (Figure S19, Supporting Information). The fast and reversible magnetic actuation into a helical shape under a 75 mT out-of-plane magnetic field is shown in Figure 5b (Video S4, Supporting Information). When applying a magnetic field and IR heating (≈80 °C) simultaneously, the actuated helical shape gradually releases its internal stress due to the bond exchange in the polymer network (Figure 5c). Upon removing the magnetic field and the heating source after ≈15 min, a stress-free 3D helical architecture with self-adjusted magnetization is formed. The reshaped helical architecture also comes with bistability, which can be triggered either by magnetic actuation or mechanical loading (Figure 5d and Video S4, Supporting Information). Such a 3D architecture would be very challenging to manufacture but can be easily achieved using our MDP approach. We conduct tensile tests to compare the mechanical behaviors and properties of the as-fabricated 2D design and the reshaped 3D architecture. Both structures are loaded by stretching the central point while fixing the edges, with experimental results illustrated in Figure 5e,f (also see Figure S19 and Video S5, Supporting Information). Before the reshaping process, the 2D structure is monostable, as the force (black curve) and rotation angle (red curve) is monotonically increasing with the displacement (Figure 5e). After reshaping, the 3D helical architecture exhibits bistable behavior, which is precisely characterized by the force–displacement curve from the tensile test (Figure 5f) loaded from the initial downward pop-out stable state. During loading, the architecture reaches the critical snapping point at around 14 mm displacement, and the structure quickly snaps through to the upward pop-out state at 21 mm displacement, where the force reduces to zero. Besides, the FEA simulation of the reshaped bistable 3D kirigami with the helical design is conducted to accurately predict the deformation under the tensile loadings (Figure S19, Supporting Information).

A more complicated 3D kirigami architecture based on concentric arc design with multistable states is manufactured by the same MDP stress releasing approach. Figure 5g shows the design and the as-fabricated planar kirigami geometry comprising seven layers of concentric arcs connected by hinges, which is initially magnetized in a mechanically stretched-out configuration (Figure S20, Supporting Information). Its magnetic actuation under a 100 mT out-of-plane magnetic field is shown in Figure 5h. After exposing to the IR light and an out-of-plane magnetic field for about 30 min (Figure 5i), the planar concentric arc structure transforms into a stress-free kirigami architecture with four stable states, which can be actuated by both mechanical loading and magnetic field, as illustrated in Figure 5j (also see Video S6, Supporting Information). The different mechanical behaviors before and after the reshaping process are evaluated by tensile tests with the same boundary conditions as previous (Figure S20, Supporting Information). Figure 5k shows that the initial planar kirigami is monostable. In contrast, as illustrated in Figure 5l, the reshaped 3D kirigami

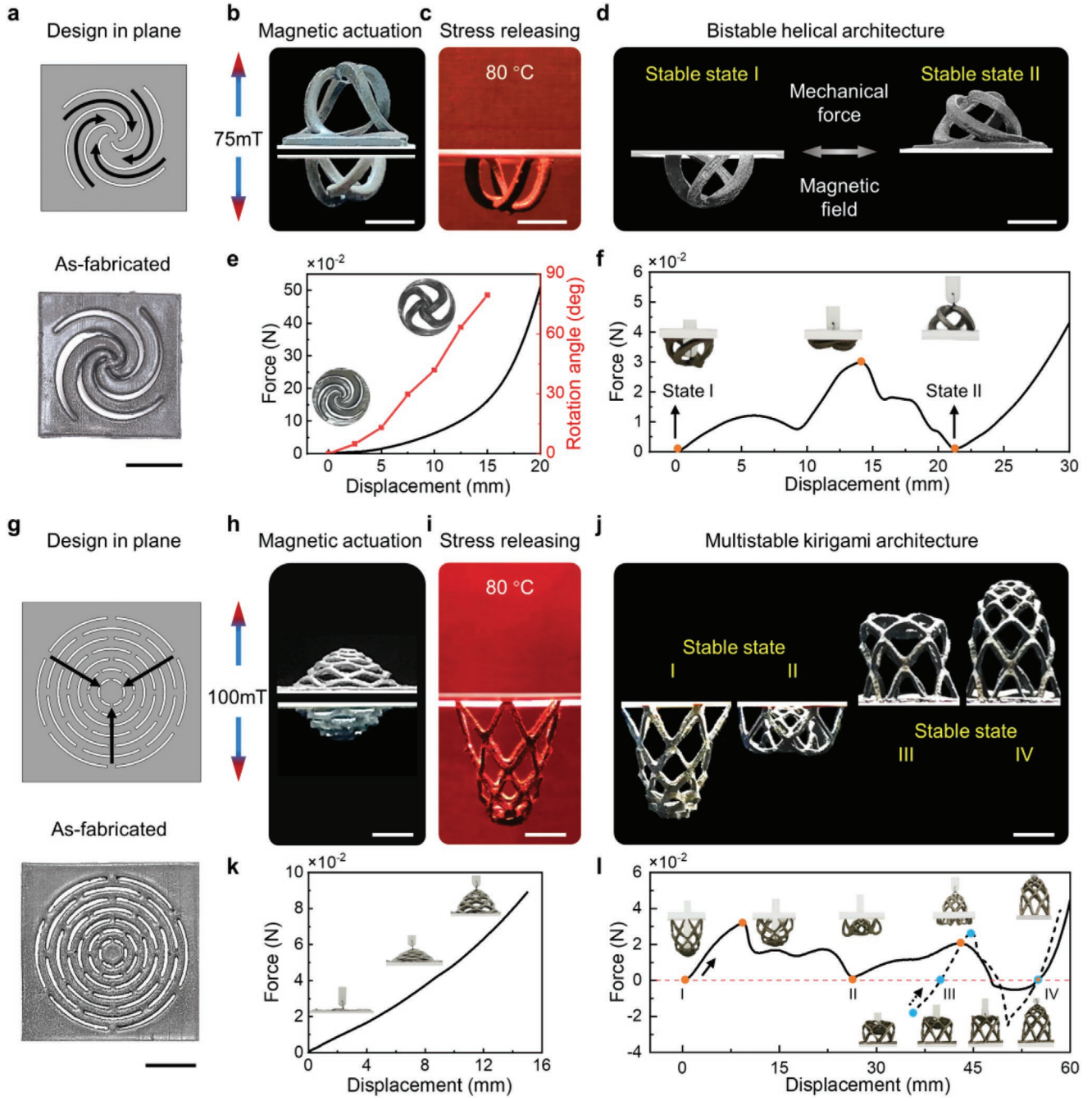

Figure 5. Magnetic-assisted permanent 3D structural reconfiguration of the MDP for manufacturing complex multistable architectures. a) Schematic design and the as-fabricated planar kirigami with helical cuts (helical design). The black arrows roughly indicate magnetization. b) Magnetic actuation of the planar helical structure. c) Stress-releasing process of the magnetic-actuated helical structure under the IR irradiation. d) Mechanical or magnetic actuation of reshaped bistable helical architecture. e,f) The force/rotation angle–displacement curves and snapshots of the helical design in tensile tests: initial planar structure (e) and reshaped 3D architecture (f). g) Schematic design and the as-fabricated planar kirigami with concentric arc cuts (concentric arc design). h) Magnetic actuation of the planar concentric arc structure. i) Stress-releasing process of the magnetic-actuated concentric arc structure under the IR irradiation. j) Images of the multistable 3D kirigami architecture with four stable states. k,l) The force–displacement curves and snapshots of the concentric arc design in tensile tests: initial planar structure (k) and reshaped 3D architecture (l). Scale bars for all images: 10 mm.

architecture has four stable states and three snapping points (marked by orange and blue circles for two loading paths) (see Figure S20 and Video S7, Supporting Information). By either magnetic actuation or mechanical stretching starting from the stable state I, two stable states II and IV are captured with two snapping points identified between states I and II, and states II and IV, respectively. This loading path is illustrated by the black solid curve and top-row insets. Note that after the architecture snaps up at the second snapping point, it compresses the load cell until reaching stable state IV. Stable state III can

be obtained from a different loading path when stretching from an intermediate compressed state, indicated by the black dashed curve and bottom-row insets of Figure 5l. This state shows an overall upward configuration with the middle part pushed down. After reaching the critical high-energy point, the middle part snaps up, and the architecture achieves stable state IV (Video S7, Supporting Information). The configurations of the reshaped 3D kirigami during mechanical actuation are also predicted by the FEA simulations (Figure S20, Supporting Information). It is worth mentioning that the MDP reshaping-enabled manufacturing of complex 3D structures is not limited to only permanent 2D-to-3D transformations. Stress-free 3D-to-3D shape reconfiguration of structures with similar topology can also be achieved by the same reshaping concept (Figure S21, Supporting Information). The manufacturing of complex 3D structures is often achieved by molding or 3D printing, after which the shape cannot be reconfigured for other functionalities. To our best knowledge, this is the first time that complex 3D architectures are manufactured through simple remotely controlled shape morphing of 2D and 3D structures.

Finally, the abovementioned functionalities of MDP, including modular assembling and welding, in situ magnetization reprogramming, and permanent structural reshaping, can be integrated with magnetic-driven remote navigation for augmented functionality and multifunctional shape morphing. Here, MDP modules can be assembled into a structure using remotely applied magnetic fields and welded by remotely applied laser. The assembled structure can be expanded with more modules to increase the functionality. The magnetization can also be reprogrammed to alter the functionality. In this approach, all the operations can be done remotely, which significantly improves the application potential of MDPs in harsh environments with limited access.

As shown in **Figure 6**a, the MDP module's locomotion can be precisely controlled by a 3D magnetic field (Figure S22, Supporting Information) to remotely assist the module assembling. Based on the logics in Figure 3, two types of modules, a single-directional magnetized module and a bidirectional magnetized module, are used to be assembled into a functional pattern. For the bidirectional magnetized module, its zero net magnetization leads to negligible motion under the small magnetic field and is thus naturally set as the fixed target. We then set the single-directional magnetized module as the free module due to its easy manipulation under a small magnetic field (≈3 mT). The magnetic-driven remote navigation is realized by two types of motions of the free module, its out-of-plane and in-plane rotations. When the free module is far from the target position, an out-of-plane rotating magnetic field is applied to cyclically rotate the free module toward the target module. By controlling the frequency and rotating axis of the external field, the speed and moving direction of the free module can be well-controlled. When the module is approaching the fixed target, an in-plane magnetic field is applied to slightly adjust the direction of the free module so that it aligns well with the target. Once the single free module is close enough to the fixed target, the magnetic attractive force will instantaneously connect the free module with the target based on the assembling logics presented in Figure 3d.

Taking advantage of this magnetic-driven remote navigation, together with the integrated multifunctionality of the MDPs, remotely controlled modular assembling and welding, magnetization reprogramming, and permanent reshaping are demonstrated (Figure 6b–d). We first create the magnetic-assisted assembly I with a strip shape (Figure 6b). The magnetic-driven remote navigation and assembling process is shown in Figure 6e, where the free modules are gathered toward the fixed target one by one with the agile control of the 3D magnetic field (assemble blocks 1–4 one-by-one). It should be noted that the magnetic field required to control the free module's locomotion is very small (3 mT), so the assembly will not deform obviously during the multiple assembling steps. Additionally, the integrity of the assembled structure will not be influenced by the applied small magnetic field as the attractive force between the modules is strong enough to hold the shape (Video S8, Supporting Information). After assembling, an IR laser pointing to each jointing seam for about 30 s can achieve good welding of the modules. The assembled strip can provide symmetric bending deformation under an upward or downward magnetic field (Figure S23, Supporting Information). As shown in Figure 6f,g, a dynamic crawling motion is demonstrated under a changing magnetic field (Figure S24, Supporting Information). The applied magnetic field has a small angle with respect to the vertical direction so that it induces an asymmetric touching area of the front end and back end with the ground, permitting a forward movement. Due to the unique feature of MDPs, it becomes possible to carry out on-the-fly modifications to the fabricated MDP structures based on needs. For example, four additional modules (blocks 5–8) can be assembled onto the previous assembly to create the magnetic-assisted assembly II with a cross shape (Figure 6c). Similarly, free modules are guided to their target positions one by one via magnetic-driven navigation (Figure 6h and Video S8, Supporting Information). After being treated with IR laser, the assembled modules are welded to an intact piece. Under the application of the upward/downward magnetic fields, the four beams bend up and down with the same deformation mode (Figure 6i and Figure S23, Supporting Information). By applying a clockwise rotating magnetic field (Figure S24, Supporting Information), the structure shows a translational movement via rolling (Figure 6j and Video S8, Supporting Information). The actuation can be reprogrammed into various deformation modes and motions by rationally designing in situ magnetization reprogramming. For example, to obtain the object transferring capability, the four ends of the cross shape structure are reprogrammed with an out-of-plane magnetization (Figure 6d), which creates an inner space under the applied magnetic field for object storage (Figure 6k). The structure morphs into two different deformation modes under the application of upward/downward magnetic fields (Figure S23, Supporting Information). As shown in Figure 6l (see Video S8, Supporting Information), while still possessing the rolling capability, a new function of encapsulating and releasing an object is integrated into the structure to achieve object transfer from one place to another under the controlled magnetic field (Figure S24, Supporting Information). By heating the actuated 2D structure at 80 °C for about 15 min, a new stress-free 3D structure can be obtained as shown in Figure 6m.

The MDP's merits are emphasized through its covalent adaptive network and magnetic-responsive feature. Comparing with previous shape morphing materials, MDPs stand out with

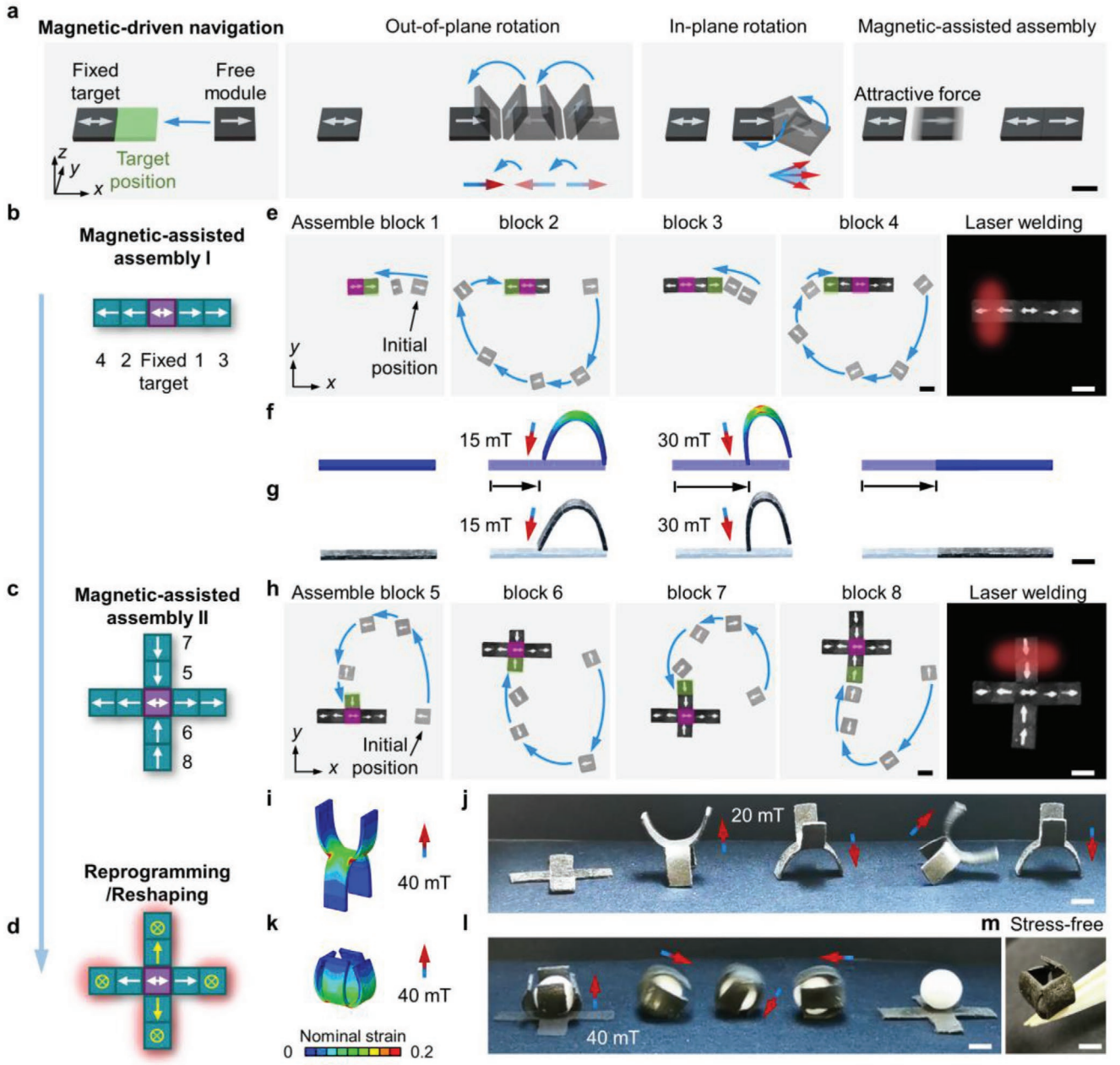

Figure 6. Magnetic-driven remote navigation and assembling of the MDP modules with combined functions for reprogrammable actuations and reconfigurable architectures. a) Mechanism of the magnetic-driven remote navigation and assembling of the MDP modules. b,c) Assembling logics of MDP modules for strip shape (b) and cross shape (c). d) Magnetization reprogramming and reshaping. e) Assembly of the strip structure in (b). f,g) Finite-element analysis (f) and an experimental demonstration of the dynamic crawling motion (g) of the assembled strip structure in (b). h) Assembly of the cross structure in (c). i,j) Finite-element analysis (i) and an experimental demonstration of dynamic rotating motion (j) of the assembled cross structure in (c). k,l) Finite-element analysis (k) and an experimental demonstration of dynamic motions (l) of the cross structure with a reprogrammed magnetization in (d) for the encapsulating and rolling motion that transfers a sphere under a clockwise rotating magnetic field. m) Permanent structural reconfiguration of the cross structure after reprogramming and reshaping. Scale bars for all images: 6 mm.

excellent performance such as untethered, fast, and reversible actuation, as well as highly desirable functionalities, including welding, reprogramming, reconfiguring, and recycling. Moreover, MDPs enable a new manufacturing approach to fabricate functional stress-free 3D architectures. Therefore, the unique performance can distinguish MDPs from the existing shape morphing materials and other MSMs.[8a,26]

3. Conclusion

We report a MDP composite to create structures with complex geometry and magnetization distribution for modular assembling and reconfigurable shape morphing architectures. The DP network rearrangement and the magnetic dipole realignment are tuned by cooperative control of the temperature field

and the magnetic field. Functional properties and applications, including seamless welding of modular assembly with targeted functional actuation, magnetization reprogramming for reconfigurable actuation modes, and remote-controlled structural reconfiguration with unusual properties, are demonstrated. The concept of the MDP by merging covalent adaptive network polymers and magnetic materials can be extended to diverse MSMs, using various stimuli-responsive dynamic reactions and numerous magnetic materials, with tunable mechanical, rheological, and magnetic properties. As the covalent adaptive network polymers enable the unique performance of material welding and structural reconfiguration in manufacturing, healing during service, and recycling at the end of service,[27] they provide a green material matrix for MSMs with enhanced multifunctionality beyond reconfigurable shape morphing. We envision the MDP and its derived functions offer great potentials for next-generation multifunctional assemblies, reconfigurable shape morphing architectures, and devices.

4. Experimental Section

Furan-Grafted Prepolymer Synthesis: 50 g of poly(ethylene glycol) diglycidyl ether (average molecular weight: 500 g mol^{-1}) (epoxy oligomer) and 9.7 g of furfurylamine (as a chain extender) in the stoichiometric ratio were mixed in 15 g of dimethylformamide (DMF), and 0.374 g of 2,6-di-*tert*-butyl-4-methylphenol (as an antioxidant) was added to the above solution in a round bottle flask. After degassing under vacuum for 5 min, the mixture was sealed for the reaction with magnetic stirring at 80 °C for 20 h and then 110 °C for another 4 h before cooling down. The obtained viscous light yellow solution was stored at room temperature before use. For prepolymer characterization, the solution was dried in a vacuum oven at 70 °C for 24 h. All reagents were purchased from Sigma-Aldrich (St. Louis, MO, USA) without further purification.

Dynamic Polymer and Magnetic Dynamic Polymer Preparation: DP was prepared by cross-linking the furan-grafted prepolymer with bismaleimide cross-linker (Sigma-Aldrich, St. Louis, MO, USA). Briefly, linear prepolymer solution (containing 20 wt% of DMF solvent) and bismaleimide with various maleimide to furan ratios (r) were manually mixed at room temperature. To manufacture MDP, 15 vol% NdFeB microparticles (134.0 wt% to the polymer matrix; Magnequench, Singapore) with an average size of 25 µm were added into the prepolymer and cross-linker mixture (with $r = 0.15$) followed by manually mixing to obtain a homogeneous blend. The resin and composite resin were poured on a poly(tetrafluoroethylene) (Teflon, PTFE, McMaster-Carr, Elmhurst, IL, USA) film. The curing was conducted with precuring at 50 °C for around 60 min to form a soft gel and then post-treated in a vacuum oven at 60 °C for one day to remove most of the solvent. To obtain films with controlled thickness, the samples were hot compressed at 110 °C with spacers between PTFE films. The samples were cooled down and stored at room temperature for at least 1 day before characterization. The materials were post-magnetized with an initial configuration under impulse magnetic fields (1.5 T) generated by an in-house built impulse magnetizer.

Characterization: The uniaxial tensile tests, dynamic thermomechanical measurements, and stress relaxation tests were performed on a DMA tester (Q800, TA Instruments, New Castle, DE, USA) using rectangular samples (dimension: about 25 × 4 × 0.9 mm). In the uniaxial tension tests, the strain rate was 0.5 min^{-1} and three specimens were tested for each type of the samples for reporting the average results. The Young's modulus was calculated by the secant modulus at 0.5% strain. DMA testing was conducted using a constant oscillation amplitude of 30 µm, a frequency of 1 Hz, and a force track of 125%. The temperature was ramped from –60 to 120 °C at a heating rate of 3 °C min^{-1}. In the stress-relaxation experiments, the samples were equilibrated at a predetermined temperature for 10 min, and then a constant strain of 2% was applied to monitor the evolution of stress as a function of time. DSC testing was measured on a Q200 DSC (TA Instruments, New Castle, DE, USA) using T-zero aluminum pans under a nitrogen purge. The testing temperature ranges from –80 to 150 °C with a heating and cooling rate of 5 °C min^{-1}. Optical microscopy images were obtained on a 7X-90X Jewelry Gem Stereo Microscope (Amscope, Irvine, CA, USA). The temperature field of samples during heating was captured using a Seek Thermal CompactPRO thermal image camera (Tyrian Systems, Inc., Santa Barbara, CA, USA). The magnetic actuation of 2D and 3D structures was conducted in a pair of in-house built electromagnetic coils with a uniform central magnetic field up to 105 mT.

Finite-Element Analysis: The shape actuations of MDP architectures and array under external magnetic fields were simulated using a user-defined element subroutine implemented in the FEA software ABAQUS 2019 (Dassault System, Dassault System, Providence, RI, USA). The input parameters used were: Young's modulus $E = 400$ kPa for MDP and $E = 130$ kPa for silicone rubber, the bulk modulus $K = 400$ MPa (approximate incompressibility), the magnetizations of the post-magnetized MDP, $M_r = 75$ kA m^{-1}, and reprogrammed MDP, $M_r = 62$ kA m^{-1} (15 vol% of magnetic particles), and the uniform external magnetic field.

Supporting Information

Supporting Information is available from the Wiley Online Library or from the author.

Acknowledgements

X.K., S.W., and Q.Z. contributed equally to this work. R.Z., S.W., Q.Z., and Y.J. acknowledge support from NSF Career Award CMMI-1943070 and NSF Award CMMI-1939543. H.J.Q., X.K., S.M.M., and L.Y. acknowledge the support of AFOSR grants (FA9550-19-1-0151 and FA9550-20-1-0306; Dr. B.-L. "Les" Lee, Program Manager) and an Office of Naval Research grant (N00014-20-1-2586). F.Y. acknowledges the support from US Department of Energy under Grant No. DE-SC0001304 (magnetization characterization). This work was performed in part at the Georgia Tech Institute for Electronics and Nanotechnology, a member of the National Nanotechnology Coordinated Infrastructure, which is supported by the National Science Foundation (ECCS-1542174).

Conflict of Interest

The authors declare no conflict of interest.

Data Availability Statement

The data that support the findings of this study are available from the corresponding author upon reasonable request.

Keywords

covalent adaptive polymers, magnetic soft materials, modular assembly, reconfigurable architecture, shape morphing

Received: March 17, 2021
Revised: April 30, 2021
Published online:

[1] a) L. Hines, K. Petersen, G. Z. Lum, M. Sitti, *Adv. Mater.* **2017**, *29*, 1603483; b) J. Yuan, W. Neri, C. Zakri, P. Merzeau, K. Kratz, A. Lendlein, P. Poulin, *Science* **2019**, *365*, 155.

[2] a) M. Wehner, R. L. Truby, D. J. Fitzgerald, B. Mosadegh, G. M. Whitesides, J. A. Lewis, R. J. Wood, *Nature* **2016**, *536*, 451; b) Z. Wang, K. Li, Q. He, S. Cai, *Adv. Mater.* **2019**, *31*, 1806849; c) L. S. Novelino, Q. Ze, S. Wu, G. H. Paulino, R. Zhao, *Proc. Natl. Acad. Sci. USA* **2020**, *117*, 24096.

[3] a) S. Xu, Z. Yan, K.-I. Jang, W. Huang, H. Fu, J. Kim, Z. Wei, M. Flavin, J. McCracken, R. Wang, *Science* **2015**, *347*, 154; b) R. Liu, X. Kuang, J. Deng, Y.-C. Wang, A. C. Wang, W. Ding, Y.-C. Lai, J. Chen, P. Wang, Z. Lin, H. J. Qi, B. Sun, Z. L. Wang, *Adv. Mater.* **2018**, *30*, 1705195; c) G. Yun, S.-Y. Tang, S. Sun, D. Yuan, Q. Zhao, L. Deng, S. Yan, H. Du, M. D. Dickey, W. Li, *Nat. Commun.* **2019**, *10*, 1300.

[4] a) A. Lendlein, R. Langer, *Science* **2002**, *296*, 1673; b) S. Fusco, M. S. Sakar, S. Kennedy, C. Peters, R. Bottani, F. Starsich, A. Mao, G. A. Sotiriou, S. Pané, S. E. Pratsinis, *Adv. Mater.* **2014**, *26*, 952; c) B. Mostaghaci, O. Yasa, J. Zhuang, M. Sitti, *Adv. Sci.* **2017**, *4*, 1700058; d) Y. Liu, J. Li, S. Song, J. Kang, Y. Tsao, S. Chen, V. Mottini, K. McConnell, W. Xu, Y.-Q. Zheng, J. B. H. Tok, P. M. George, Z. Bao, *Nat. Biotechnol.* **2020**, *38*, 1031; e) A. Ghosh, L. Li, L. Xu, R. P. Dash, N. Gupta, J. Lam, Q. Jin, V. Akshintala, G. Pahapale, W. Liu, *Sci. Adv.* **2020**, *6*, eabb4133.

[5] a) M. Behl, M. Y. Razzaq, A. Lendlein, *Adv. Mater.* **2010**, *22*, 3388; b) Y. Liu, J. K. Boyles, J. Genzer, M. D. Dickey, *Soft Matter* **2012**, *8*, 1764; c) Q. Ge, C. K. Dunn, H. J. Qi, M. L. Dunn, *Smart Mater. Struct.* **2014**, *23*, 094007; d) A. Lendlein, O. E. C. Gould, *Nat. Rev. Mater.* **2019**, *4*, 116.

[6] a) A. S. Gladman, E. A. Matsumoto, R. G. Nuzzo, L. Mahadevan, J. A. Lewis, *Nat. Mater.* **2016**, *15*, 413; b) H. Banerjee, M. Suhail, H. Ren, *Biomimetics* **2018**, *3*, 15; c) K. Liu, Y. Zhang, H. Cao, H. Liu, Y. Geng, W. Yuan, J. Zhou, Z. L. Wu, G. Shan, Y. Bao, Q. Zhao, T. Xie, P. Pan, *Adv. Mater.* **2020**, *32*, 2001693.

[7] a) T. J. White, D. J. Broer, *Nat. Mater.* **2015**, *14*, 1087; b) T. H. Ware, M. E. McConney, J. J. Wie, V. P. Tondiglia, T. J. White, *Science* **2015**, *347*, 982.

[8] a) V. Q. Nguyen, A. S. Ahmed, R. V. Ramanujan, *Adv. Mater.* **2012**, *24*, 4041; b) J. C. Breger, C. Yoon, R. Xiao, H. R. Kwag, M. O. Wang, J. P. Fisher, T. D. Nguyen, D. H. Gracias, *ACS Appl. Mater. Interfaces* **2015**, *7*, 3398; c) S. Wu, W. Hu, Q. Ze, M. Sitti, R. Zhao, *Multifunct. Mater.* **2020**, *3*, 042003.

[9] a) J. Rahmer, C. Stehning, B. Gleich, *Sci. Rob.* **2017**, *2*, eaal2845; b) W. Hu, G. Z. Lum, M. Mastrangeli, M. Sitti, *Nature* **2018**, *554*, 81; c) Y. Kim, G. A. Parada, S. Liu, X. Zhao, *Sci. Rob.* **2019**, *4*, eaax7329.

[10] R. Zhao, Y. Kim, S. A. Chester, P. Sharma, X. Zhao, *J. Mech. Phys. Solids* **2019**, *124*, 244.

[11] a) G. Z. Lum, Z. Ye, X. Dong, H. Marvi, O. Erin, W. Hu, M. Sitti, *Proc. Natl. Acad. Sci. USA* **2016**, *113*, E6007; b) X. Dong, G. Z. Lum, W. Hu, R. Zhang, Z. Ren, P. R. Onck, M. Sitti, *Sci. Adv.* **2020**, *6*, eabc9323; c) S. Wu, Q. Ze, R. Zhang, N. Hu, Y. Cheng, F. Yang, R. Zhao, *ACS Appl. Mater. Interfaces* **2019**, *11*, 41649.

[12] a) J. Kim, S. E. Chung, S.-E. Choi, H. Lee, J. Kim, S. Kwon, *Nat. Mater.* **2011**, *10*, 747; b) T. Xu, J. Zhang, M. Salehizadeh, O. Onaizah, E. Diller, *Sci. Rob.* **2019**, *4*, eaav4494.

[13] a) Y. Kim, H. Yuk, R. Zhao, S. A. Chester, X. Zhao, *Nature* **2018**, *558*, 274; b) S. Wu, C. M. Hamel, Q. Ze, F. Yang, H. J. Qi, R. Zhao, *Adv. Intell. Syst.* **2020**, *2*, 2000060.

[14] a) E. Diller, C. Pawashe, S. Floyd, M. Sitti, *Int. J. Rob. Res.* **2011**, *30*, 1667; b) H. Gu, Q. Boehler, D. Ahmed, B. J. Nelson, *Sci. Rob.* **2019**, *4*, eaax8977; c) K. Han, C. W. Shields IV, B. Bharti, P. E. Arratia, O. D. Velev, *Langmuir* **2020**, *36*, 7148.

[15] E. Diller, N. Zhang, M. Sitti, *J. Micro-Bio Rob.* **2013**, *8*, 121.

[16] a) Q. Ze, X. Kuang, S. Wu, J. Wong, S. M. Montgomery, R. Zhang, J. M. Kovitz, F. Yang, H. J. Qi, R. Zhao, *Adv. Mater.* **2020**, *32*, 1906657; b) J. Cui, T.-Y. Huang, Z. Luo, P. Testa, H. Gu, X.-Z. Chen, B. J. Nelson, L. J. Heyderman, *Nature* **2019**, *575*, 164; c) Y. Alapan, A. C. Karacakol, S. N. Guzelhan, I. Isik, M. Sitti, *Sci. Adv.* **2020**, *6*, eabc6414; d) M. Li, Y. Wang, A. Chen, A. Naidu, B. S. Napier, W. Li, C. L. Rodriguez, S. A. Crooker, F. G. Omenetto, *Proc. Natl. Acad. Sci. USA* **2018**, *115*, 8119; e) H. Song, H. Lee, J. Lee, J. K. Choe, S. Lee, J. Y. Yi, S. Park, J.-W. Yoo, M. S. Kwon, J. Kim, *Nano Lett.* **2020**, *20*, 5185; f) H. Deng, K. Sattari, Y. Xie, P. Liao, Z. Yan, J. Lin, *Nat. Commun.* **2020**, *11*, 6325.

[17] a) Z. Fang, H. Song, Y. Zhang, B. Jin, J. Wu, Q. Zhao, T. Xie, *Matter* **2020**, *2*, 1187; b) J. Deng, X. Kuang, R. Liu, W. Ding, A. C. Wang, Y.-C. Lai, K. Dong, Z. Wen, Y. Wang, L. Wang, H. J. Qi, T. Zhang, Z. L. Wang, *Adv. Mater.* **2018**, *30*, 1705918; c) Z. P. Zhang, M. Z. Rong, M. Q. Zhang, *Prog. Polym. Sci.* **2018**, *80*, 39.

[18] a) A. Gandini, *Prog. Polym. Sci.* **2013**, *38*, 1; b) X. Chen, M. A. Dam, K. Ono, A. Mal, H. Shen, S. R. Nutt, K. Sheran, F. Wudl, *Science* **2002**, *295*, 1698.

[19] a) M. Podgórski, B. D. Fairbanks, B. E. Kirkpatrick, M. McBride, A. Martinez, A. Dobson, N. J. Bongiardina, C. N. Bowman, *Adv. Mater.* **2020**, *32*, 1906876; b) W. Zou, J. Dong, Y. Luo, Q. Zhao, T. Xie, *Adv. Mater.* **2017**, *29*, 1606100.

[20] a) X. Lu, S. Guo, X. Tong, H. Xia, Y. Zhao, *Adv. Mater.* **2017**, *29*, 1606467; b) G. Zhang, W. Peng, J. Wu, Q. Zhao, T. Xie, *Nat. Commun.* **2018**, *9*, 4002; c) B. Jin, H. Song, R. Jiang, J. Song, Q. Zhao, T. Xie, *Sci. Adv.* **2018**, *4*, eaao3865; d) X. Kuang, Q. Mu, D. J. Roach, H. J. Qi, *Multifunct. Mater.* **2020**, *3*, 045001.

[21] R. S. Sahu, Y.-l. Cheng, Y.-f. Su, Y.-h. Shih, *J. Taiwan Inst. Chem. Eng.* **2020**, *116*, 137.

[22] X. Kuang, G. Liu, X. Dong, D. Wang, *Mater. Chem. Front.* **2017**, *1*, 111.

[23] K. Yu, N. X. Fang, G. Huang, Q. Wang, *Adv. Mater.* **2018**, *30*, 1706348.

[24] a) A. Nasto, P. M. Reis, *J. Appl. Mech.* **2014**, *81*, 121008; b) M. A. Dias, C. D. Santangelo, *Europhys. Lett.* **2012**, *100*, 54005; c) J. L. Silverberg, A. A. Evans, L. McLeod, R. C. Hayward, T. Hull, C. D. Santangelo, I. Cohen, *Science* **2014**, *345*, 647; d) L. Jin, A. E. Forte, B. Deng, A. Rafsanjani, K. Bertoldi, *Adv. Mater.* **2020**, *32*, 2001863.

[25] a) S. J. Callens, A. A. Zadpoor, *Mater. Today* **2018**, *21*, 241; b) G. P. T. Choi, L. H. Dudte, L. Mahadevan, *Nat. Mater.* **2019**, *18*, 999; c) C. Ma, S. Wu, Q. Ze, X. Kuang, R. Zhang, H. J. Qi, R. Zhao, *ACS Appl. Mater. Interfaces* **2020**, *13*, 12639; d) S. M. Montgomery, S. Wu, X. Kuang, C. D. Armstrong, C. Zemelka, Q. Ze, R. Zhang, R. Zhao, H. J. Qi, *Adv. Funct. Mater.* **2020**, *31*, 2005319.

[26] X. Kuang, D. J. Roach, C. M. Hamel, K. Yu, H. J. Qi, *Multifunct. Mater.* **2020**, *3*, 032002.

[27] a) C. E. Diesendruck, N. R. Sottos, J. S. Moore, S. R. White, *Angew. Chem., Int. Ed.* **2015**, *54*, 10428; b) J. F. Patrick, M. J. Robb, N. R. Sottos, J. S. Moore, S. R. White, *Nature* **2016**, *540*, 363; c) N. Zheng, Y. Xu, Q. Zhao, T. Xie, *Chem. Rev.* **2021**, *121*, 1716.